# Upscaling energy concentration in multifrequency single-bubble sonoluminescence with strongly degassed sulfuric acid

Damián Dellavale, Ludmila Rechiman, Juan Manuel Rosselló, and Fabián Bonetto
*Instituto Balseiro-CONICET, Centro Atómico Bariloche, Río Negro, R8402AGP, Argentina*
(Received 6 April 2012; revised manuscript received 3 June 2012; published 20 July 2012)

Single-bubble sonoluminescence (SBSL) was explored under a variety of multifrequency excitations. In particular, biharmonic excitation was used to produce SBSL for unprecedented low dissolved noble gas concentrations in a sulfuric acid solution. Reducing the amount of dissolved noble gas makes it possible to reach higher acoustic pressures on the SL bubble, which otherwise are not attainable because of the Bjerknes instability. By using biharmonic excitation, we were able to experimentally trap and to spatially stabilize SL bubbles for xenon pressure overhead as low as 1 mbar. As a result, we have access to regions in phase space where the plasma temperatures are higher than the ones reached before for bubbles driven at ≈30 kHz.

DOI: 10.1103/PhysRevE.86.016320 PACS number(s): 78.60.Mq

## I. INTRODUCTION

It has long been known that, in order to increase energy concentration in single-bubble sonoluminescence (SBSL), avoiding the abrupt extinction of the SL bubble (Rayleigh-Taylor and parametric shape instabilities), increasing the acoustic pressure on the bubble ($P_{\mathrm{LF},b}$) while keeping the SL bubble at the resonator center (positional stability), and decreasing the amount of dissolved noble gases (minimum ambient radius $R_0$) are needed [1–3]. However, to access the regions of parameter space with minimum $R_0$ and maximum $P_{\mathrm{LF},b}$ has proven to be a challenge to the experimentalist. Flannigan and Suslick [4] used a sulfuric acid (SA) aqueous solution that allowed a significant increase in luminescence. One of the limiting mechanisms of energy concentration upscale in SA is the positional instability of the SL bubble. We showed that, due to the mean primary Bjerknes force, the bubble reaches a position where the acoustic pressure is always the same irrespective of the pressure in the center of the resonator [5]. A further noteworthy complication of SBSL in SA originates from the movement of the SL bubble in quasiperiodic orbits (spatial instability) [6,7]. Toegel *et al.* [7] showed that the history force is responsible for the orbits. Urteaga and Bonetto [8] suppressed the orbits using a biharmonic (two frequencies) excitation. In this paper, we have used an aqueous solution that is 85% sulfuric acid by weight (SA85) since its high viscosity prevents Rayleigh-Taylor shape instability. We also used a very low concentration of noble gas (xenon pressure overhead of 1 mbar) to investigate the regions of parameter space $R_0 - P_{\mathrm{LF},b}$ where the high maximum bubble temperatures ($T_{\max}$) are expected (minimum $R_0$, maximum$P_{\mathrm{LF},b}$) [1–3]. Using a particular biharmonic driving, we achieved unprecedented low $R_0$ and high $P_{\mathrm{LF},b}$ upscaling the energy concentration at the bubble collapse. Under these conditions, the computed plasma temperatures are higher than those achieved for bubbles driven with single-frequency (≈30 kHz).

## II. APPARATUS

We used a spherical flask made of quartz (60 mm in outer diameter and approximately 1 mm in thickness). In all cases presented here the liquid was SA85. The multifrequency driving was applied through four PZT drivers glued on the flask. Two opposed PZT drivers were used for the low-frequency driving ($V_{\mathrm{LF}}$ at $f_0$), and the other two PZTs were used for the high-frequency driving ($V_{\mathrm{HF}}$) similar to the arrangement in Ref. [8]. In all the experiments described below, we used, as the fundamental frequency, the one corresponding to the resonator first mode ($f_0 \approx 29.2$ kHz). We developed a tailored system for concurrent signal synthesis and measurement based on field programmable gate array (FPGA) technology [9,10]. The high-frequency signal ($V_{\mathrm{HF}}$) was amplified using a custom-built low distortion high voltage amplifier ($B_w = 400$ kHz at $C_L = 2$ nF) to excite the high-frequency drivers. A small piezoelectric ceramic microphone was glued to the resonator wall in order to obtain a signal proportional to the applied acoustic pressure at the center of the resonator ($P_{\mathrm{LF}}$). We also detected the SL pulse using an Oriel 77340 phototube. The use of a timer (Stanford Research Systems SR620) allowed us to measure the time of collapse ($t_c$), defined as the time interval between the acoustic pressure zero crossing with negative slope and the SL pulse arrival. The time precision of the measurements was only limited by the microphone signal jitter to about 100 ns. The timer was operated at its maximum rate (≈1500 samples/s). The SL intensity, stability, and position of the SL bubble within the resonator were provided by a CCD camera (Hitachi KPF120). To measure the bubble radius temporal evolution [$R(t)$], we used conventional Mie light scattering techniques [11]. In order to determine all the quantities of interest, the Mie scattering data were matched to a simulation obtained with a state-of-the-art model described in Ref. [12] (and references therein).

## III. SPATIAL INSTABILITY

In order to prevent the errors of the Mie scattering data caused by the bubble pseudo-orbits, we produced spatially stable SL bubbles using one of the two mechanisms: (1) We produced almost fixed SL bubbles at the resonator center by using single-frequency driving ($f_0$) and low $P_{\mathrm{LF}}$ [zone *(A)* in the left photograph of Fig. 3). (2) Alternatively, we remove the spatial instability using harmonic excitation ($Nf_0$), ranging from $N = 3$ (≈88 kHz) to $N = 7$ (≈205 kHz) besides the

 

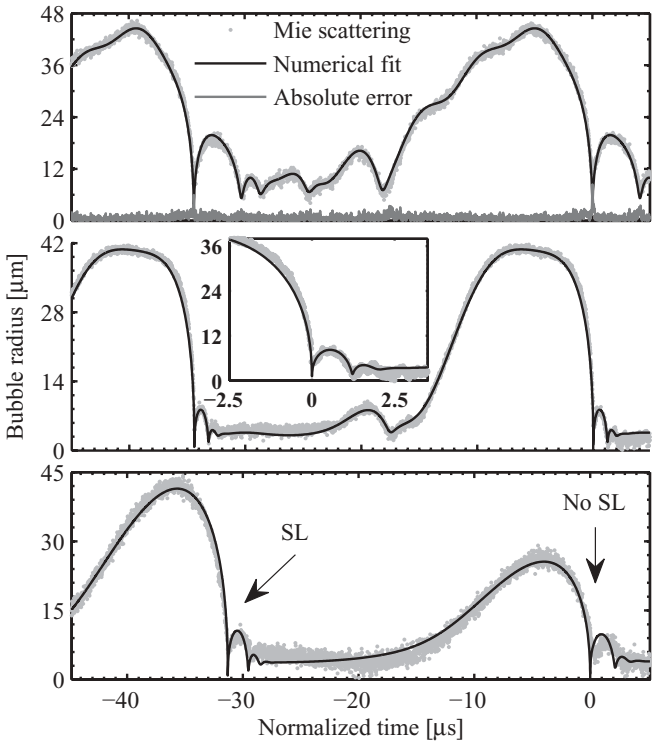


FIG. 1. Bubble radius temporal evolution from Mie scattering data (argon SL bubbles in SA85). The data points are the phototube signal (ten averaged traces) converted to a signal proportional to the bubble radius. The solid black curve is the best numerical fit using the numerical model. Upper graph: Spatially stabilized SL bubble by using biharmonic driving with the seventh harmonic ($f_0$ and $7f_0 \approx 204$ kHz). Fitted parameters: ambient bubble radius $R_0 = 10.8$ $\mu$m, low-frequency acoustic pressure $P_{\mathrm{LF},b} = 1.19$ bar, high-frequency acoustic pressure $P_{\mathrm{HF},b} = 1.17$ bar, and relative phase $\phi = +1.58$ $\mu$s (positive when the high frequency is advanced with respect to the low frequency). The computed maximum bubble temperature is $T_{\max} = 8.4$ kK. The concentration of argon dissolved in SA85 is $c_\infty/c_{\mathrm{sat}} = 0.033$, where $c_\infty$ and $c_{\mathrm{sat}}$ are the ambient and saturation gas concentrations, respectively. Middle graph: Spatially stabilized SL bubble by using biharmonic driving with the fourfold harmonic ($f_0$ and $4f_0 \approx 116$ kHz). Fitted parameters: $R_0 = 4.7$ $\mu$m, $P_{\mathrm{LF},b} = 1.51$ bar, $P_{\mathrm{HF},b} = 0.8$ bar, and $\phi = -2.5$ $\mu$s, resulting in $T_{\max} = 33$ kK and $c_\infty/c_{\mathrm{sat}} = 0.003$. Lower graph: SL bubble driven by a bifrequency (not harmonic) excitation ($f_0$ and 44.1 kHz). Fitted parameters: $R_0 = 5.4$ $\mu$m, $P_{\mathrm{LF},b} = 1.35$ bar, and $P_{\mathrm{HF},b} = 0.19$ bar, resulting in $T_{\max} = 26.7$ kK and $c_\infty/c_{\mathrm{sat}} \approx 0.006$.

fundamental frequency ($f_0$). By virtue of the real-time processing capability of the FPGA-based hardware [9,10], we were able to perform active suppression of the largest harmonic observed in the microphone signal ($12f_0 \approx 350$ kHz). This harmonic was produced by the acoustic emission of the SL bubble. During the active suppression of the harmonic, the spatial stability, $R(t)$ and $t_c$ of the SL bubble were not significantly changed. The spatial stability and the dynamics [$R(t)$] of the SL bubble were only affected when harmonic excitation was applied with amplitudes much larger than those produced by the acoustic emission of the SL bubble. Figure 1 shows the Mie scattering data and the best numerical fit for spatially stable SL bubbles (away from the resonator center). For the case of single-frequency (not shown) and biharmonic excitations, the agreement between the experimental results and the model is excellent. Not only biharmonic, but also bifrequency (not harmonic) excitations were explored. Thus, period doubling on the $R(t)$ was observed under bifrequency excitation (lower panel of Fig. 1). Nevertheless, the bifrequency (not harmonic) excitation seems to not directly stimulate the energy focusing in SBSL.

## IV. RELATIVE PHASE

In case of the biharmonic excitation, the exploration of the relative phase ($\alpha$) between the fundamental ($V_{\mathrm{LF}}$ at $f_0$) and harmonic ($V_{\mathrm{HF}}$ at $Nf_0$) excitations has been performed that exploits the tuning capabilities of our FPGA-based hardware [9,10]. Thus, we measured the time of collapse ($t_c$) and the bubble position (radial direction $r_b$ and azimuthal angle $\theta_b$) within the spherical resonator as a function of the relative phase ($\alpha$). Figure 2 shows the typical behavior of the measured $r_b$, $\theta_b$, and $t_c$ values as a function of the relative phase $\alpha$. We found that, as the relative phase ($\alpha$) is increased,

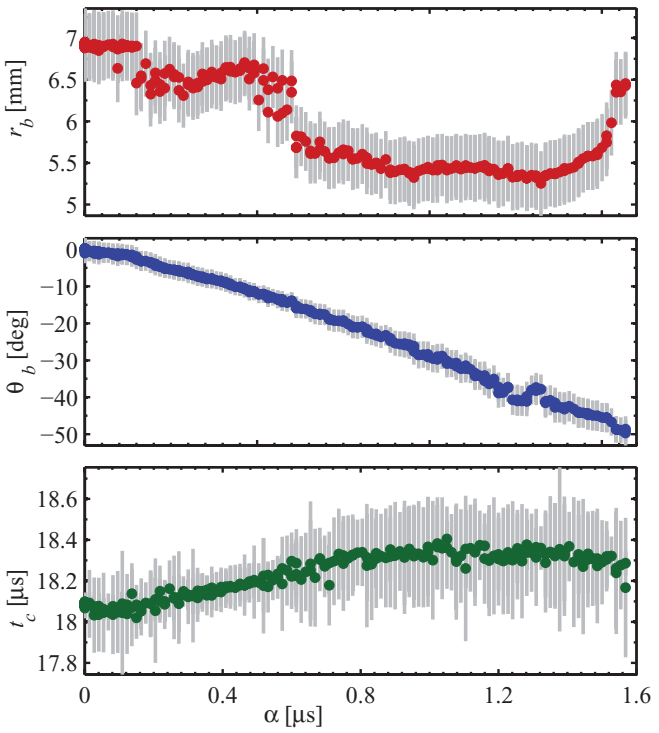


FIG. 2. (Color online) Experimental data for the SL bubble position and time of collapse ($t_c$) as a function of the relative phase ($\alpha$) between the fundamental ($V_{\mathrm{LF}}$ at $f_0$) and the harmonic ($V_{\mathrm{HF}}$ at $7f_0 \approx 204$ kHz) excitations. The measurement was performed with $\approx$20 mbar of argon pressure head dissolved in SA85. The range of excursion of $\alpha$ was $T/3 \approx 1.6$ $\mu$s, where $T = 1/(7f_0) \approx 5$ $\mu$s is the period of the harmonic excitation. Upper graph: Bubble position within the spherical resonator along the radial direction $r_b$. Middle graph: Bubble position within the spherical resonator along the azimuthal angle $\theta_b$. For $r_b \approx 6$ mm and $\Delta\theta_b \approx 50^\circ$, the arc length is $\approx$5 mm. Lower graph: Time of collapse ($t_c$) of the SL bubble. The error bars of $t_c$ are the standard deviation of $\approx$400 measurements at each point.

the main displacement of the SL bubble occurs along the azimuthal angle ($\theta_b$). It is worth noting that the latter suggests a nonradially symmetric vibration of the spherical resonator, i.e., excitation of resonance modes $j_{l,n}$ without radial symmetry $l > 0$ (where $j_{l,n}$ is the $l$-order spherical Bessel function) [10,13]. Although sudden bubble displacements were observed during the ramp of $\alpha$, their sporadic natures suggest that they are related to the complex acoustic environment of the SL bubble rather than the relative phase $\alpha$. Before the ramp of $\alpha$ was applied, we tuned the amplitudes ($V_{\mathrm{LF}}$ and $V_{\mathrm{HF}}$) and relative phase ($\alpha$) in order to obtain a spatially stable SL bubble. During the ramp of $\alpha$, the standard deviation in the $t_c$ values (error bars in Fig. 2) increase when the SL bubble starts describing orbits. More importantly, Fig. 2 shows that, during the ramp of $\alpha$, the time of collapse ($t_c$) was not significantly changed.

Using the Mie scattering technique, measurements of the $R(t)$ were performed on a spatially stable SL bubble for different values of the relative phase $\alpha$ (the SL bubble was set at different positions away from the resonator center for each $\alpha$ value). Rather remarkably, from the experimental data [$R(t)$], it was found that the relative phase $\phi$ on the bubble (between $P_{\mathrm{LF},b}$ and $P_{\mathrm{HF},b}$) seems to be the same regardless of the relative phase $\alpha$ value (between $V_{\mathrm{LF}}$ and $V_{\mathrm{HF}}$) of the biharmonic driving. For a spatially stable SL bubble, when the relative phase ($\alpha$) is changed, the bubble moves (mainly along the azimuthal angle $\theta_b$) to a new stable position where $\phi$, $R(t)$, and $t_c$ are kept almost unchanged. Thus, the relative phase $\phi$ on the bubble (between $P_{\mathrm{LF},b}$ and $P_{\mathrm{HF},b}$) could not be settled arbitrarily by varying the relative phase $\alpha$ (between $V_{\mathrm{LF}}$ and $V_{\mathrm{HF}}$) of the biharmonic driving. Experimentally, it was found that the relative phase ($\alpha$) has a poor effect on $\phi$, $R(t)$, and $t_c$. These results show that, due to the positional instability along the azimuthal angle $\theta_b$, the effectiveness of the relative phase ($\alpha$) to directly stimulate the energy focusing in SBSL is quite limited.

## V. POSITIONAL INSTABILITY: BJERKNES FORCE INSTABILITY

A set of measurements was performed to explore the positional instability [5] under a variety of biharmonic excitations: We trap a single SL bubble next to the resonator center. At this point, we activated the high-frequency driving ($V_{\mathrm{HF}} \approx 160\ V_{\mathrm{RMS}}$) corresponding to the preconfigured harmonic ($Nf_0$). We acquired the amplitude of the microphone signal, the time of collapse ($t_c$), and the bubble position within the resonator as a function of $V_{\mathrm{LF}}$ with a constant amplitude of the high-frequency driving ($V_{\mathrm{HF}} \approx 160\ V_{\mathrm{RMS}}$). The amplitude of the low-frequency driving was varied from the onset of SL, at about $P_{\mathrm{LF}} = 1.2$ bar, until the bubble was located near the resonator wall at about $P_{\mathrm{LF}} = 2.6$ bar. In addition, another set of similar runs was performed using single-frequency driving ($V_{\mathrm{HF}} = 0$). For bubbles at the resonator center, the combination of the experimental Mie scattering data [$R(t)$] with the numerical model allowed us to obtain the acoustic pressure on the bubble ($P_{\mathrm{LF},b}$) and to calibrate the filtered microphone signal. In particular, the microphone signal was used to obtain the range of the acoustic pressure ($1.2\ \mathrm{bar} \leqslant P_{\mathrm{LF}} \leqslant 2.6\ \mathrm{bar}$, see Figs. 3 and 5) produced by the ramps of the low-frequency driving ($150 V_{\mathrm{RMS}} \leqslant V_{\mathrm{LF}} \leqslant 350 V_{\mathrm{RMS}}$). Photographs in Fig. 3

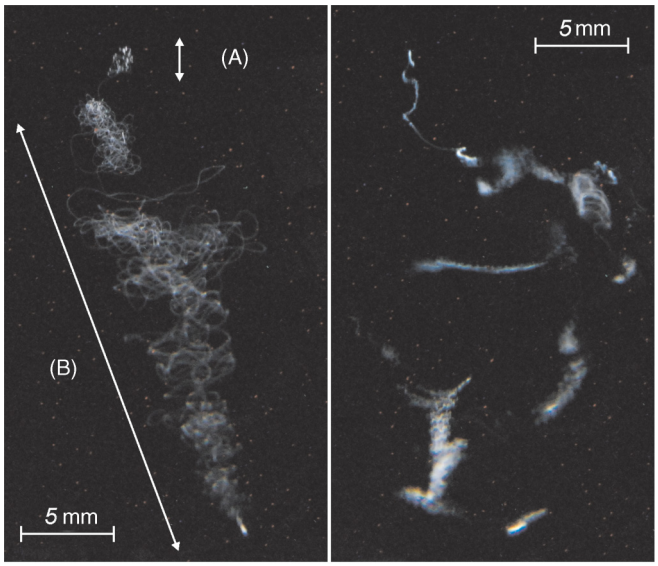


FIG. 3. (Color online) Photographs (30 s exposure) of SL bubbles in the Ar-SA85 system for a ramp of $P_{\mathrm{LF}}$ ($1.2\ \mathrm{bar} \leqslant P_{\mathrm{LF}} \leqslant 2.6\ \mathrm{bar}$). Left: Single-frequency driving ($f_0$). Right: Biharmonic driving ($f_0$ and $7f_0 \approx 204$ kHz at $V_{\mathrm{HF}} \approx 160\ V_{\mathrm{RMS}}$).

illustrate the typical behavior of the SL bubble during the ramps of $P_{\mathrm{LF}}$. Under single-frequency driving (left photograph in Fig. 3) and low enough $P_{\mathrm{LF}}$ [$P_{\mathrm{LF}} \leqslant 1.5$ bar, zone *(A)*], the SL bubble is almost fixed (without orbits) next to the resonator center (pressure antinode). As the $P_{\mathrm{LF}}$ is further increased, the SL bubble shifts from the pressure antinode and simultaneously starts describing orbits [$P_{\mathrm{LF}} \gg 1.5$ bar, zone *(B)*]. In the latter case, the $t_c$ and $P_{\mathrm{LF},b}$ reach maximum constant values [5]. The history force [7] together with the Bjerknes force instability [5] account for the observed behavior under single-frequency driving (left photograph in Fig. 3). On the other hand, by adding a harmonic excitation besides the ramp of $P_{\mathrm{LF}}$, we observed abrupt transitions in the $t_c$ and $P_{\mathrm{LF},b}$ values brought about by sudden displacements of the SL bubble along its path toward the resonator wall (right photograph in Fig. 3). However, the parameters $t_c$ and $P_{\mathrm{LF},b}$ tend to monotonically increase with the ramp of $P_{\mathrm{LF},b}$, until they reach maximum constant values. We argue that the sudden displacements of the SL bubble are caused by the pressure nodes and antinodes of the high-frequency mode excited by the harmonic driving. Nevertheless, it is important to note that, in order to account for the observed behavior of the SL bubble, the following dynamics have to be taken into account: (1) bubble radius temporal evolution [$R(t)$], (2) translational motion of the bubble (pseudo-orbits) and, (3) resonances and frequency response of the acoustic resonator [10,13].

Figure 4 shows the plane $P_{\mathrm{LF},b} - R_0$ for the Ar-SA85 system in the case of a single-frequency driving. Figure 4 also shows the observed $t_c$ lower (unfilled square) and upper ($t_c|_{\max}$: filled square) bounds measured during the ramp of $P_{\mathrm{LF}}$ at $c_\infty/c_{\mathrm{sat}} = 0.012$.

The upper graph of Fig. 5 shows the $t_c$ excursions (vertical bars) produced by the $P_{\mathrm{LF}}$ ramps. The $t_c$ excursions were measured by adding different harmonic excitations ($V_{\mathrm{HF}} \approx 160\ V_{\mathrm{RMS}}$ at $Nf_0$) besides the ramp of $P_{\mathrm{LF}}$ ($1.2\ \mathrm{bar} \leqslant P_{\mathrm{LF}} \leqslant 2.6$ bar at $f_0$). The gray (red) triangles shown in the upper

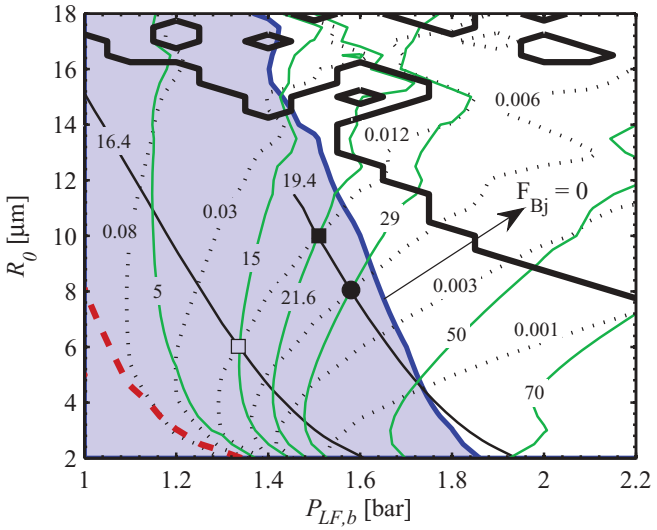


FIG. 4. (Color online) Computed $P_{LF,b} - R_0$ parameter space for the Ar-SA85 system in the case of a single-frequency driving ($f_0 \approx 29.2$ kHz). The thick dashed line (red) is the Blake threshold [2]. Thick filled line (black) corresponds to the parametric shape instability threshold shown together with the Rayleigh-Taylor shape instability for the mode $n = 2$. The dotted curves are the equilibrium bubble states ($c_\infty/c_{sat}$ = cte). The thin filled curves (green) are the contours of $T_{max}$ (in units of kK). The thin black curves are the contours of $t_c$ (in units of microseconds). The filled (unfilled) square corresponds to the maximum (minimum) $t_c$ value measured during the ramp of $P_{LF}$ at $c_\infty/c_{sat} = 0.012$. The filled square ($t_c = 19.4$ μs) defines the upper end of the $t_c$ bar for $N = 1$ in Fig. 5. Thick filled line (blue) is the Bjerknes stability threshold. The time of collapse at the Bjerknes stability threshold is $t_c = 20.1$ μs. The experimental data point (•) corresponds to a spatially stable SL bubble with fitted parameters: $R_0 = 8.1$ μm and $P_{LF,b} = 1.58$ bar, resulting in $T_{max} = 29$ kK and $c_\infty/c_{sat} = 0.006$.

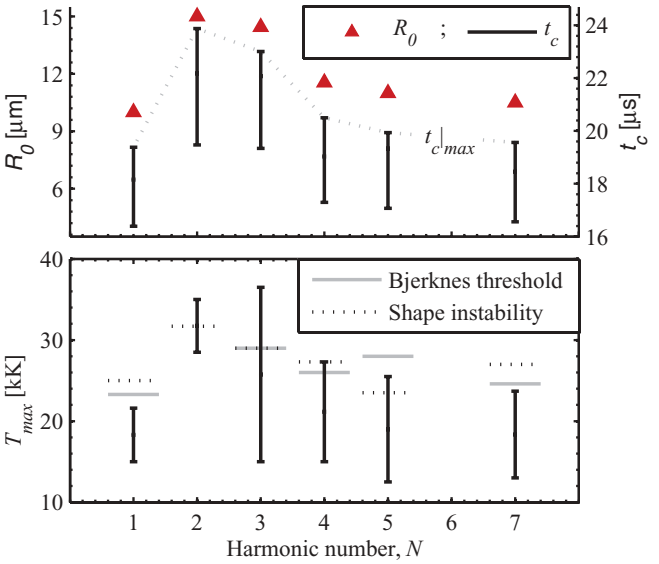


FIG. 5. (Color online) Upper graph, vertical bars: Experimental $t_c$ excursions measured with different harmonic excitations ($Nf_0$) besides the ramp of $P_{LF}$. The harmonic $Nf_0$ added in each run is shown in the abscissa of the lower panel. The $t_c$ excursions were obtained as the average of five independent $P_{LF}$ ramps. The $t_c$ excursion at $N = 1$ corresponds to a single-frequency driving ($V_{HF} = 0$, see Fig. 4). For $N > 1$ (biharmonic excitation), the amplitude of the high-frequency driving was $V_{HF} \approx 160 V_{RMS}$. In all of the cases, the range of the ramps was 1.2 bar $\leqslant P_{LF} \leqslant$ 2.6 bar, and the argon pressure head dissolved in SA85 was ≈12 mbar. The data points ▲ (red) are the $R_0$ values, computed by using the numerical model, corresponding to the observed $t_c$ upper bound ($t_c|_{max}$). Lower graph, vertical bars: Excursions of $T_{max}$ computed from the observed $t_c$ during the ramps of $P_{LF}$. The filled gray lines are the computed $T_{max}$ at the Bjerknes instability threshold. The dotted black lines are the computed $T_{max}$ at the shape instability threshold for the mode $n = 2$.

graph of Fig. 5 are the $R_0$ values corresponding to the maximum $t_c$ ($t_c|_{max}$) observed experimentally. We found that the observed $t_c|_{max}$ values are in good agreement with the computed Bjerknes instability threshold. The Bjerknes threshold corresponds to the points in the $P_{LF,b} - R_0$ plane in which the mean primary Bjerknes force becomes zero [$F_{Bj} = 0$, where $F_{Bj} = -(4\pi/3T)\int_T \nabla P(r,t) R^3(t) dt$ and $T = 1/f_0$] [5]. Using the numerical model [12], we perform extensive computations of the $F_{Bj}$ in the $P_{LF,b} - R_0$ plane for the biharmonic excitations explored in the experiments. Thus, the experimental $t_c|_{max}$ values measured at the end of the ramps of $P_{LF}$ are very close (slightly above or below) the computed $t_c|_{max}$ values at the Bjerknes instability threshold. Furthermore, the difference between the computed and the measured $t_c|_{max}$ values does not exceed 10% for both single-frequency and biharmonic drivings. Using the numerical model [12], we converted the measured range of excursions of $t_c$ to values of the maximum bubble temperature ($T_{max}$). The lower graph of Fig. 5 shows the $T_{max}$ excursions during the ramps of $P_{LF}$. Besides, the lower graph also shows the $T_{max}$ upper bound as predicted by the Bjerknes (filled gray line) and shape (dotted black line) instability thresholds.

We want to point out that in the case of the harmonic $N = 2$ (Fig. 5), the SL bubble was located near the resonator wall for the entire range of the $P_{LF}$ ramp. The numerical model [12] was used in order to account for this behavior. We found that, for the biharmonic excitation with $N = 2$, the region of parameter space numerically explored (1.1 bar $\leqslant P_{LF} \leqslant$ 2.2 bar; 2 μm $\leqslant R_0 \leqslant$ 18 μm) is Bjerknes unstable. Moreover, the observed spreading of the $t_c$ values (vertical bar for $N = 2$ shown in the upper graph of Fig. 5) was due to period-doubling regimes and a series of sudden drops in $t_c$ rather than a monotonic increase during the $P_{LF}$ ramp. Urteaga *et al.* [14] (and references therein), reported similar burst and sudden transitions in $t_c$ associated with the recycling mode for SBSL in water under single-frequency driving. Even though these results for biharmonic driving ($N = 2$) suggest that the pinch-off of the bubble could have taken place (shape instability), we never observed an abrupt disappearance of the bubble. We argue that, if the bubble is broken into pieces, these fragments recombine to form a new bubble with a renewed intake of noble gas avoiding the SL bubble extinction. These results suggest that, for SBSL in SA85 with single-frequency and biharmonic drivings, the parametric shape instabilities set limits for the parameter space of SBSL towards large ambient bubble radii ($R_0 > 15$ μm, see Fig. 4 and upper graph of Fig. 5 for $N = 2$). On the other hand, toward low dissolved noble gas

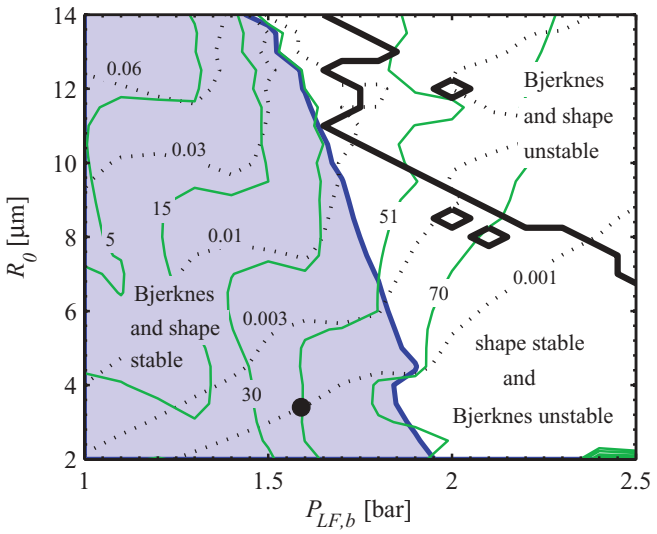


FIG. 6. (Color online) Computed $P_{\mathrm{LF},b} - R_0$ parameter space for the Xe-SA85 system in the case of a biharmonic driving ($f_0$, $4f_0 \approx 116$ kHz). The dotted thin curves are the equilibrium bubble states ($c_\infty/c_{\mathrm{sat}} = \mathrm{cte}$). The thin filled curves (green) are the contours of $T_{\max}$ (in units of kK). Thick filled line (black) corresponds to the parametric shape instability threshold shown together with the Rayleigh-Taylor shape instability for the mode $n = 2$. Thick filled line (blue) is the Bjerknes stability threshold. The experimental data point (•) corresponds to a spatially stable SL bubble with fitted parameters $R_0 = 3.4$ $\mu$m, $P_{\mathrm{LF},b} = 1.59$ bar, $P_{\mathrm{HF},b} = 1.18$ bar, and $\phi = -2.9$ $\mu$s, resulting in $T_{\max} \approx 51$ kK. For this condition ($c_\infty/c_{\mathrm{sat}} \approx 0.001$), the Bjerknes threshold limits the $T_{\max}$ to about 70 kK.

concentrations in SA85 ($c_\infty/c_{\mathrm{sat}} < 0.01$), the Rayleigh-Taylor shape instability occurs at larger acoustic pressures ($P_{\mathrm{LF},b}$) than those for the Bjerknes force instability (see Figs. 4 and 6). Therefore, for low dissolved noble gas concentrations in SA85 ($c_\infty/c_{\mathrm{sat}} < 0.01$), the Bjerknes force instability determines the mean radial position of the SL bubble within the resonator and prevents access to higher $P_{\mathrm{LF},b}$ for both single-frequency and biharmonic drivings.

For the data shown in Fig. 5 ($c_\infty/c_{\mathrm{sat}} \approx 0.012$), the SL intensities were obtained with the CCD camera slightly defocused to prevent saturation. We found similar SL intensities for the harmonics $N = 4,5,7$ and higher SL intensities for the cases $N = 2,3$. The $t_c|_{\max}$ values shown in Fig. 5 were measured at the end of the ramps of $P_{\mathrm{LF}}$ for which the SL bubble was next to the resonator wall. Using a calibrated detector (Newport 840-C) located next to the resonator wall, we also measured the SL intensity $I_{\mathrm{SL}}$ (referred to $\lambda = 400$ nm) corresponding to the observed $t_c$ upper bound ($t_c|_{\max}$). Thus, in the case of high order harmonics ($N = 4,5,7$), the SL intensity was $I_{\mathrm{SL}} \approx 0.7$ $\mu$W. On the other hand, the harmonics $N = 3$ and $N = 2$ produced $I_{\mathrm{SL}} \approx 1.3$ $\mu$W and $I_{\mathrm{SL}} \approx 3.6$ $\mu$W, respectively. The model predicts that the enhancement of $I_{\mathrm{SL}}$ (and $t_c$), in the case of low order harmonics ($N = 2,3$), correlates with the increasing in the ambient bubble radius ($R_0$) (see Fig. 5). Hopkins *et al.* [6] found that, in SBSL with SA, the enhancement in the emitted light is accompanied by an increase in both the flash width and the ambient bubble radius ($R_0$), whereas, the expansion ratio ($R_{\max}/R_0$) and the calculated Rayleigh-Plesset maximum collapse velocity ($\dot{R}_{\max}$) are diminished. The decrease in the $R_{\max}/R_0$ as well as in the $\dot{R}_{\max}$ implies that the bubble implosion becomes remarkably weaker. On the other hand, the increase in the ambient bubble radius ($R_0$) and the flash width suggest an increase in the size of the emitting core during the collapse. Moreover, the shape of the Bjerknes instability threshold in the $P_{\mathrm{LF},b} - R_0$ plane (see Figs. 4 and 6), indicates that higher acoustic pressures ($P_{\mathrm{LF},b}$) are available only at small ambient radii (i.e., very low dissolved noble gas concentrations in the fluid $c_\infty/c_{\mathrm{sat}} \ll 0.01$). As a consequence, increasing the $T_{\max}$ involves using very low $c_\infty/c_{\mathrm{sat}}$ (small $R_0$) where the Bjerknes instability allows one to reach higher $P_{\mathrm{LF},b}$. Besides, in the case of small $R_0$, the SL intensity ($I_{\mathrm{SL}}$) becomes significantly weaker due to the small size of the emitting plasma core.

## VI. UPSCALING ENERGY CONCENTRATION

Other than $T_{\max}$, the suitable parameters to assess the intensity of the bubble main collapse are the expansion ratio $R_{\max}/R_0$ [2] and the maximum collapse velocity $\dot{R}_{\max}$ [2,6]. The computed maximum bubble temperature ($T_{\max}$) sensitively depends on the detailed description of the emitting core (i.e., physical plasma properties), whereas, the parameters $R_{\max}/R_0$ and $\dot{R}_{\max}$ do not. More importantly, the latter parameters are determined by the bubble dynamics [$R(t)$]. In this respect, the agreement between the experimental results and our numerical model [12] are excellent for both single-frequency and biharmonic excitations (see Fig. 1). In particular, the timing and the relative amplitude of the rebounds are in very good agreement between the experiment and the numerical model. Table I summarizes the fitted ($R_0, P_{\mathrm{LF},b}$) and the computed ($T_{\max}, \dot{R}_{\max}, R_{\max}/R_0$) parameters of the SL bubbles experimentally observed for the lowest dissolved noble gas concentrations achieved in our experiments with SA85.

We want to point out that, for similar $P_{\mathrm{LF},b}$ values, reducing the ambient bubble radius $R_0$ with increasing the expansion relation $R_{\max}/R_0$ implies a more violent bubble collapse [2], which in turn, leads to more energy per quasiparticles (molecules or atoms) inside the bubble. This behavior ($R_{\max}/R_0$ and $R_0$) is consistent with the values of $\dot{R}_{\max}$ and $T_{\max}$ shown in Table I. From the comparison of the parameters $T_{\max}$, $\dot{R}_{\max}$, $R_{\max}/R_0$, and $R_0$ between the cases with single

TABLE I. Parameters of the SL bubbles observed for the lowest dissolved noble gas concentrations achieved in our experiments with SA85.

| | $T_{\max}$ (kK) | $\dot{R}_{\max}$ (m/s) | $\frac{R_{\max}}{R_0}$ | $R_0$ ($\mu$m) | $P_{\mathrm{LF},b}$ (bar) |
|---|---|---|---|---|---|
| Single-frequency driving, Ar-SA85: $c_\infty/c_{\mathrm{sat}} = 0.006$, (Filled black circle in Fig. 4). | 29 | 718 | 7 | 8.1 | 1.58 |
| Bi-harmonic driving, Ar-SA85: $c_\infty/c_{\mathrm{sat}} = 0.003$, (Middle graph of Fig. 1). | 33 | 1031 | 9 | 4.7 | 1.51 |
| Bi-harmonic driving, Xe-SA85: $c_\infty/c_{\mathrm{sat}} = 0.001$, (Filled black circle in Fig. 6). | 51 | 1320 | 12.1 | 3.4 | 1.59 |

and biharmonic drivings (Table I), it can be seen that all of them show the same trend: A more violent bubble collapse occurs in the case of biharmonic excitation (second and third cases in Table I). The consistency among the parameters $T_{\max}$, $\dot{R}_{\max}$, $R_{\max}/R_0$, and $R_0$, together with the agreement between the numerical model and the experimental results, are strong evidence that the biharmonic excitation allows for access to regions in phase space where the energy concentration is upscaled. Furthermore, in the case of single-frequency driving (first case in Table I), these regions ($c_\infty/c_{\text{sat}} < 0.005$) of phase space were not attainable because of the Bjerknes force instability. In the case of single-frequency driving (Fig. 4), the lower the $c_\infty/c_{\text{sat}}$, the higher the $P_{\text{LF},b}$ required to reach the stable diffusive equilibrium $[\partial(c_\infty/c_{\text{sat}})/\partial R_0|_{\dot{m}=0} > 0]$ [2]. Using single-frequency driving, we could not produce SBSL at gas concentrations lower than ≈5 mbar. When high driving voltage was used for $c_\infty/c_{\text{sat}} < 0.005$ (even at the maximum voltage allowed by the actuators $V_{\text{LF}} \approx 700 V_{\text{RMS}}$), the seed bubble rapidly moved toward the resonator wall (positional instability) where $P_{\text{LF},b}$ decreased significantly. For single-frequency driving and $c_\infty/c_{\text{sat}} \approx 0.005$ (see Fig. 4), the Bjerknes instability sets a limit of $T_{\max} \approx 33$ kK, $\dot{R}_{\max} = 815$ m/s, $R_{\max}/R_0 \approx 7.4$, $R_0 = 8.2\ \mu$m, and $P_{\text{LF},b} \approx 1.65$ bar. On the other hand, the phase diagrams for biharmonic excitation (e.g., Fig. 6) show that the curves of diffusive equilibrium are stable (positively sloped) even at low $P_{\text{LF},b}$. Employing the same system (resonator and driver) and biharmonic excitation ($f_0$ and $4f_0$), we were able to experimentally trap and to spatially stabilize SL bubbles in Xe-SA85 systems for xenon pressure head as low as 1 mbar. Figure 6 shows the experimental data point in the computed $P_{\text{LF},b} - R_0$ parameter space for the Xe-SA85 system in the case of a fourfold harmonic besides the fundamental frequency. The data point represents the fitted parameters ($R_0$, $P_{\text{LF},b}$, $P_{\text{HF},b}$, and $\phi$) for the spatially stable SL bubble. Figure 6 shows that the $T_{\max}$ for the spatially stable SL bubble is ≈51 kK. For this condition ($c_\infty/c_{\text{sat}} \approx 0.001$), the Bjerknes instability sets an upper bound of $T_{\max} \approx 70$ kK, $\dot{R}_{\max} = 1734$ m/s, $R_{\max}/R_0 \approx 12.1$, $R_0 = 4.3\ \mu$m, and $P_{\text{LF},b} \approx 1.85$ bar.

## VII. CONCLUSIONS

We have showed that biharmonic excitation is a mechanism that makes it possible to trap and to spatially stabilize SL bubbles in SA85 for very low $c_\infty/c_{\text{sat}}$. Thus, we reached regions of parameter space with low $R_0$, high $R_{\max}/R_0$ and $P_{\text{LF},b}$, were the intensity of the bubble collapse is upscaled. In the case of single-frequency driving these conditions were not attainable because of the Bjerknes force instability. Using biharmonic excitation (Fig. 6), we were able to produce SBSL with $c_\infty/c_{\text{sat}}$ lower by about a factor of 5 and a mechanical energy density $P_{\text{LF},b}(R_{\max}/R_0)^3$ higher by a factor of 5 than those attainable in the case of single-frequency driving (Fig. 4). As a consequence, we achieved a twofold increase in $T_{\max}$.

## ACKNOWLEDGMENTS

We gratefully acknowledge the contribution of R. Urteaga who participated in some discussion stages of this work. D.D. acknowledges support from the CONICET. This work was partially financed by the Argentinian MinCyT.

[1] S. J. Putterman and K. Weninger, Annu. Rev. Fluid Mech. **32**, 445 (2000).
[2] M. Brenner, S. Hilgenfeldt, and D. Lohse, Rev. Mod. Phys. **74**, 425 (2002).
[3] S. Hilgenfeldt and D. Lohse, Phys. Rev. Lett. **82**, 1036 (1999).
[4] D. Flannigan and K. Suslick, Nature (London) **434**, 52 (2005).
[5] R. Urteaga, D. H. Dellavale, G. F. Puente, and F. J. Bonetto, Phys. Rev. E **76**, 056317 (2007).
[6] S. D. Hopkins, S. J. Putterman, B. A. Kappus, K. S. Suslick, and C. G. Camara, Phys. Rev. Lett. **95**, 254301 (2005).
[7] R. Toegel, S. Luther, and D. Lohse, Phys. Rev. Lett. **96**, 114301 (2006).
[8] R. Urteaga and F. J. Bonetto, Phys. Rev. Lett. **100**, 074302 (2008).
[9] D. Dellavale, M. Sonnaillon, and F. Bonetto, *IEEE 4th Southern Conference on Programmable Logic* (IEEE, Piscataway, NJ, 2008), p. 269.
[10] D. Dellavale, Ph.D. thesis, Balseiro Institute, 2012.
[11] B. P. Barber and S. J. Putterman, Phys. Rev. Lett. **69**, 3839 (1992).
[12] G. F. Puente, P. García-Martínez, and F. J. Bonetto, Phys. Rev. E **75**, 016314 (2007).
[13] D. Dellavale, R. Urteaga, and F. J. Bonetto, J. Acoust. Soc. Am. **127**, 186 (2010).
[14] R. Urteaga, D. Dellavale, G. Puente, and F. Bonetto, J. Acoust. Soc. Am. **124**, 1490 (2008).